

Pseudogap formation above the superconducting dome in iron-pnictides

T. Shimojima^{1,2,*}, T. Sonobe¹, W. Malaeb^{3,4}, K. Shinada¹, A. Chainani^{5,6}, S. Shin^{2,3,4,5},
T. Yoshida^{4,7}, S. Ideta¹, A. Fujimori^{4,7}, H. Kumigashira⁸, K. Ono⁸, Y. Nakashima⁹, H. Anzai¹⁰,
M. Arita¹⁰, A. Ino⁹, H. Namatame¹⁰, M. Taniguchi^{9,10}, M. Nakajima^{4,7,11}, S. Uchida^{4,7},
Y. Tomioka^{4,11}, T. Ito^{4,11}, K. Kihou^{4,11}, C. H. Lee^{4,11}, A. Iyo^{4,11}, H. Eisaki^{4,11}, K. Ohgushi^{3,4},
S. Kasahara^{12,13}, T. Terashima¹², H. Ikeda¹³, T. Shibauchi¹³, Y. Matsuda¹³, K. Ishizaka^{1,2}

¹ *Department of Applied Physics, University of Tokyo, Bunkyo, Tokyo 113-8656, Japan.*

² *JST, CREST, Chiyoda, Tokyo 102-0075, Japan*

³ *ISSP, University of Tokyo, Kashiwa 277-8581, Japan.*

⁴ *JST, TRIP, Chiyoda, Tokyo 102-0075, Japan*

⁵ *RIKEN SPring-8 Center, Sayo, Hyogo 679-5148, Japan*

⁶ *Department of Physics, Tohoku University, Aramaki, Aoba-ku, Sendai 980-8578, Japan*

⁷ *Department of Physics, University of Tokyo, Bunkyo, Tokyo 113-0033, Japan.*

⁸ *KEK, Photon Factory, Tsukuba, Ibaraki 305-0801, Japan.*

⁹ *Graduate School of Science, Hiroshima University, Higashi-Hiroshima 739-8526, Japan.*

¹⁰ *Hiroshima Synchrotron Center, Hiroshima University, Higashi-Hiroshima 739-0046, Japan*

¹¹ *National Institute of Advanced Industrial Science and Technology, Tsukuba 305-8568, Japan.*

¹² *Research Center for Low Temperature and Materials Sciences, Kyoto University, Kyoto 606-8502, Japan.*

¹³ *Department of Physics, Kyoto University, Kyoto 606-8502, Japan.*

In the normal state above the superconducting transition temperature (T_c), the momentum-resolved electronic structure of the high- T_c cuprate shows a depletion dubbed the pseudogap, which becomes less pronounced with doping. Its relation to the high- T_c superconductivity has been a key issue, and the possible rotational symmetry breaking in this state has been reported suggesting a peculiar electronic ordering preceding the superconducting pairing. Here we provide direct evidence for a systematic evolution of the pseudogap phase via angle-resolved photoemission spectroscopy on another family of high- T_c superconductor, iron-pnictides. We observe the P-substitution evolution of pseudogap in $\text{BaFe}_2(\text{As}_{1-x}\text{P}_x)_2$, which develops well above the magnetostructural transitions and persists above the nonmagnetic superconducting dome, showing a notable similarity with cuprates. In addition, the pseudogap formation is accompanied by inequivalent energy shifts in zx/yz orbitals of iron atoms, indicative of a peculiar iron orbital ordering which breaks the fourfold rotational symmetry.

The pseudogap (PG) observed in the normal state of the high- T_c copper oxide superconductors remains a mysterious state of matter [1-3]. It has been attributed to several mechanisms such as a precursor pairing [4-6] and a novel form of spin/charge ordering [7-9]. Nearly a quarter-century after its discovery [10], it is still extensively debated in the literature and no consensus has been reached regarding its origin. In order to gain further insights into the relationship between the high- T_c superconductivity and the PG, the exploration of the PG phase in other high- T_c superconductors is highly desired.

Iron-pnictides [11] are another class of high- T_c

superconductors whose typical phase diagram is shown in Fig. 1. The parent compound shows stripe-type antiferromagnetic (AF) ordering at T_N accompanying a lattice distortion from tetragonal to orthorhombic structure at T_s [12]. In contrast to the parent cuprate which is an AF insulator, the parent pnictide is an AF metal. The electronic structure derived from multiple Fe $3d$ orbitals [13], consists typically of disconnected hole and electron Fermi surfaces (FSs), which undergo an electronic reconstruction across T_N and T_s [14, 15]. In addition to spin fluctuations derived from the nesting between the disconnected FSs [16, 17], orbital fluctuations are also a candidate for a

driving force of electron pairing in iron-pnictides [18, 19]. The importance of the orbital degrees of freedom in the itinerant ground states attracted much attention in terms of orbital ordering, defined as an inequivalent electronic occupation of zx/yz orbitals [20-22]. Intensive researches suggested that iron-pnictides can be distinguished from copper-oxides, according to orbital multiplicity and its itinerant nature. It has been, thus, an important issue whether high- T_c iron-pnictide family exhibits a PG phase in common with cuprates.

One of the most intriguing properties of iron-pnictides recently reported is their two-fold rotational symmetry of various physical properties below $T_{N,s}$, as probed by transport [23], optical [24], scanning tunneling microscopy (STM) [25], inelastic neutron scattering [26] and ARPES measurements [14, 15]. There have been experimental reports showing the persistence of two-fold symmetries even above $T_{N,s}$ [15, 27-30]. In particular, isovalent-doping system $\text{BaFe}_2(\text{As}_{1-x}\text{P}_x)_2$ (AsP122) [31] shows that an electronic nematic phase transition, which breaks the rotational symmetry of the lattice, occurs at T_{Nem}^* well above $T_{N,s}$ and persists over the superconducting (SC) dome (Fig. 1) [27]. It should be noted that such a two-fold symmetric electronic nematic state has been reported in the PG region of high- T_c cuprates [6].

Although several studies have been reported on the PG formation [32-40], the PG phase has not been completely established in the phase-diagrams of the iron-pnictides. In particular, only a few angle-resolved photoemission spectroscopy (ARPES) studies have shown the presence of an energy gap in the momentum space in the normal state [41]. In this work, we report the precise momentum-resolved electronic structure of AsP122, in pursuit of as-yet-unknown PG phase and its relation to the electronic nematicity.

Single crystals of BaFe_2As_2 were synthesized using the flux method. The starting materials Ba, FeAs were placed in an alumina crucible. This was then sealed in a double quartz tube under 0.3 atmosphere of Ar. The tube was heated at 1273 K for 2 h, slowly cooled to 1073 K for 24 h, and then quenched to room temperature (T) [42]. Single crystals of $\text{BaFe}_2(\text{As}_{1-x}\text{P}_x)_2$ with $x = 0.07, 0.24, 0.30, 0.35, 0.45, 0.61$ were grown by a self-flux method [31,43]. The precursors of Ba_2As_3 , Ba_2P_3 , FeAs and FeP were mixed, and then sealed in a quartz tube. All the processes were carried out in a glove box filled with dry N_2 gas. The tube was heated at 1150 °C for 10 h, and slowly cooled down to 900 °C at a cooling rate 1 °C/h, followed by decanting the flux. The composition of the grown single crystals was confirmed by the energy dispersive X-ray analysis [43].

Laser-ARPES measurements were performed on a spectrometer built using a VG-Scienta R4000WAL electron analyzer and a VUV-laser of 6.994 eV [44] as a photon source at ISSP. Using the $\lambda/2$ (half-wave) plate, we can rotate the light polarization vector and obtain s - or p -polarized light without changing the optical path. The energy resolution was set to ~ 5 meV to get high count rate. ARPES measurements at Brillouin zone corner were performed using a spectrometer VG-Scienta R4000WAL electron analyzer, motor-controlled 6-axis manipulator and a Helium discharge lamp of $h\nu = 40.8$ eV at University of Tokyo. The energy resolution was set to ~ 10 meV. The spectra were reproducible over measurement cycles of 12 hours. Fermi level (E_F) of samples was referenced to that of gold film evaporated onto the sample substrate. The single crystals were cleaved at 200 K in ultra high vacuum of $\sim 5 \times 10^{-11}$ Torr. We did not observe any difference in data even when the crystals were cleaved at the lowest T . Synchrotron-based ARPES measurements were carried out at BL 9A of Hiroshima Synchrotron Radiation Center (HiSOR) and BL 28A of Photon Factory (PF). At HiSOR BL 9A, a VG-Scienta R4000 analyzer and circularly-polarized light were used with the total energy resolution of ~ 8 meV. At PF BL-28A, a VG-Scienta SES-2002 analyzer and circularly-polarized light were used with the total energy resolution of ~ 10 meV. The crystals were cleaved in situ at $T \sim 10$ K in an ultra-high vacuum of $\sim 5 \times 10^{-11}$ Torr.

AsP122 system shows quasi-two dimensional FSs above $T_{N,s}$ as shown in Fig. 2(a). Three hole-FSs and two electron-FSs exist around Brillouin zone (BZ) center and the zone corner, respectively [45]. Substituting As ions by isovalent P ion causes reduction of the pnictogen height without changing the carrier density. As P ion is doped, the warping of the outer-hole FS along k_z axis increases, resulting in the larger outer-hole FS near Z plane (Fig. 2(a)). In order to investigate the T -dependence of the fine electronic structure in the multi-orbital system, it is required to clearly separate the multiple band dispersions. For this purpose, we use laser-ARPES ($h\nu = 6.994$ eV) and detect the electronic structure at the zone center near Z plane (Fig. 2(b)) [46, 47]. By choosing the s -polarized laser as the photon source, we can successfully separate the outer hole-band from other bands (Fig. 2(c-e)), owing to the distinct orbital characters of the hole FS sheets [48] and selection rules for ARPES [49]. Here we focus on the outer hole-band for investigating its T -dependence at $x = 0.00$ ($T_{N,s} = 136$ K), 0.07 ($T_{N,s} = 114$ K) 0.24 ($T_{N,s} = 55$ K, $T_c = 16$ K), 0.30 ($T_c = 30$ K), 0.45 ($T_c = 22$ K) and 0.61 ($T_c = 9$ K) of AsP122.

Figure 3(a-c) show the T -dependence of the energy

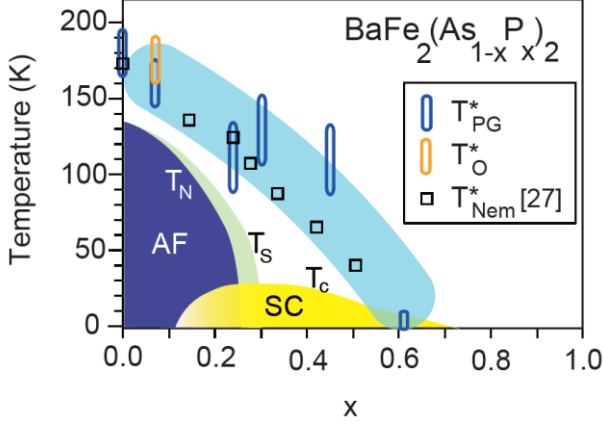


Fig. 1. Temperature-doping ($T-x$) phase diagram of $\text{BaFe}_2(\text{As,P})_2$. Blue and orange markers indicate the critical temperatures of the PG formation T_{PG}^* and inequivalent energy shift in zx/yz orbitals T_O^* obtained by laser-ARPES, respectively. Square symbols represent nematic transition temperature T_{Nem}^* obtained by torque magnetometry [27].

distribution curves (EDCs) at the Fermi momentum (k_F) in the outer hole-band at $x = 0.07, 0.30$ and 0.61 . EDCs at $x = 0.61$ clearly intersect with each other at E_F , as simply expected by the T -dependence of the Fermi-Dirac (FD) distribution (Fig. 3(c)). In contrast, EDCs at $x = 0.07$ in Fig. 3(a) exhibit drastic T -dependence below ~ 150 K. As shown in the inset, the spectral weight at the Fermi level (E_F) decreases with lowering T , indicating the evolution of a gap-like structure. Similar T -dependences are also observed for $x = 0.30$ (Fig. 3(b)), although the gap-like structure itself becomes weaker with increasing x . This result indicates that the gap-like structure exists in a wide T - and x -region, which seems to disappear toward $x \sim 0.6$.

In order to extract the intrinsic T -dependent part of the spectral weight, the EDCs are symmetrized with respect to E_F , and further normalized by the smoothed EDC recorded at the highest T (200, 170, 180 K for $x = 0.07, 0.30$ and 0.61), as shown in Fig. 3(d-f). The symmetrized EDCs for $x = 0.61$ again indicates T -independent spectral weight similar to normal metal, thus showing the accuracy and the validity of the data analysis. The symmetrized EDCs at 0.07 and 0.30 clearly show the depression of the spectral weight in the normal state. We attribute this depression to the formation of the PG.

We note that the PG appears around a certain temperature T_{PG}^* . For example, at $x = 0.07$, the symmetrized EDC at $T = 150$ K slightly shows a gap feature near E_F , while those at $T = 170$ K and 200 K remain unchanged. T_{PG}^* is thus estimated to be between 150 K and 170 K. Here we quantitatively estimate T_{PG}^*

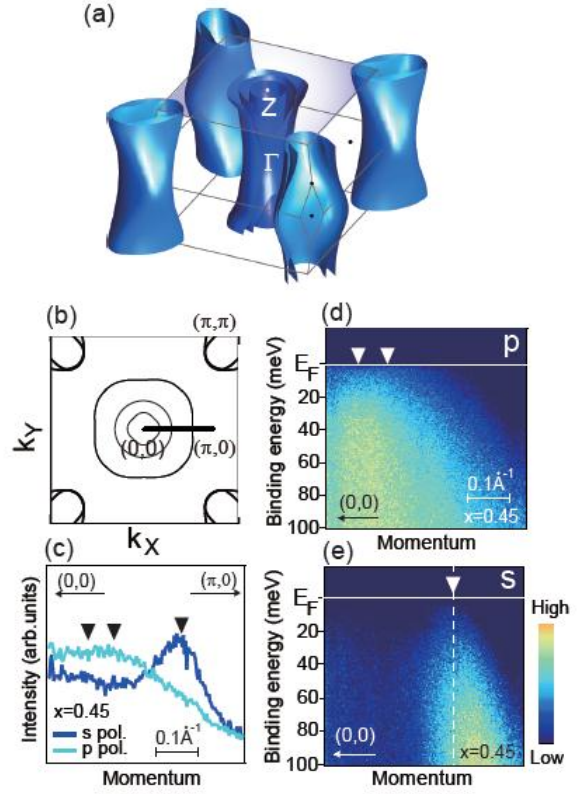


Fig. 2. (a) Calculated FSs of $\text{BaFe}_2(\text{As,P})_2$. (b) Schematics of the in-plane cut of FS sheets in Z plane of $\text{BaFe}_2(\text{As,P})_2$. X, Y in k_X and k_Y represents the tetragonal in-plane momentum axes. Black bar indicates the momentum region measured by laser-ARPES for $0.07 \leq x \leq 0.61$. The measured momentum cut for $x = 0.00$ is along $(0,0) - (\pi,\pi)$ direction. (c) Momentum distribution curves at Fermi level for $x = 0.45$ recorded by s- (blue) and p- (light blue) polarizations, along momentum cut shown in (b). Black triangles indicate the k_F for inner, middle and outer hole FSs from $(0,0)$ to $(\pi,0)$, determined by the peak positions of the momentum distribution curves. Inner- and middle- Fermi momenta are nearly degenerate. (d,e) Hole bands at $x = 0.45$ measured along the momentum cut shown in (b) by using p- and s-polarizations, respectively. Outer-hole band can be separately observed by choosing s-polarization in the experimental geometry shown in (b). The energy distribution curves in outer hole-band were obtained at the Fermi momentum as indicated by broken white line in (e).

for each P concentration. Figure 4(a-f) show the symmetrized EDCs (same as the spectra in Fig. 3(d-f)), with offsets and zero lines (horizontal black line) superimposed on respective curves as references, to focus on the T -dependent part of the spectra. The black area in each spectrum indicates the decrease of the spectral weight with lowering T , which should represent the PG formation.

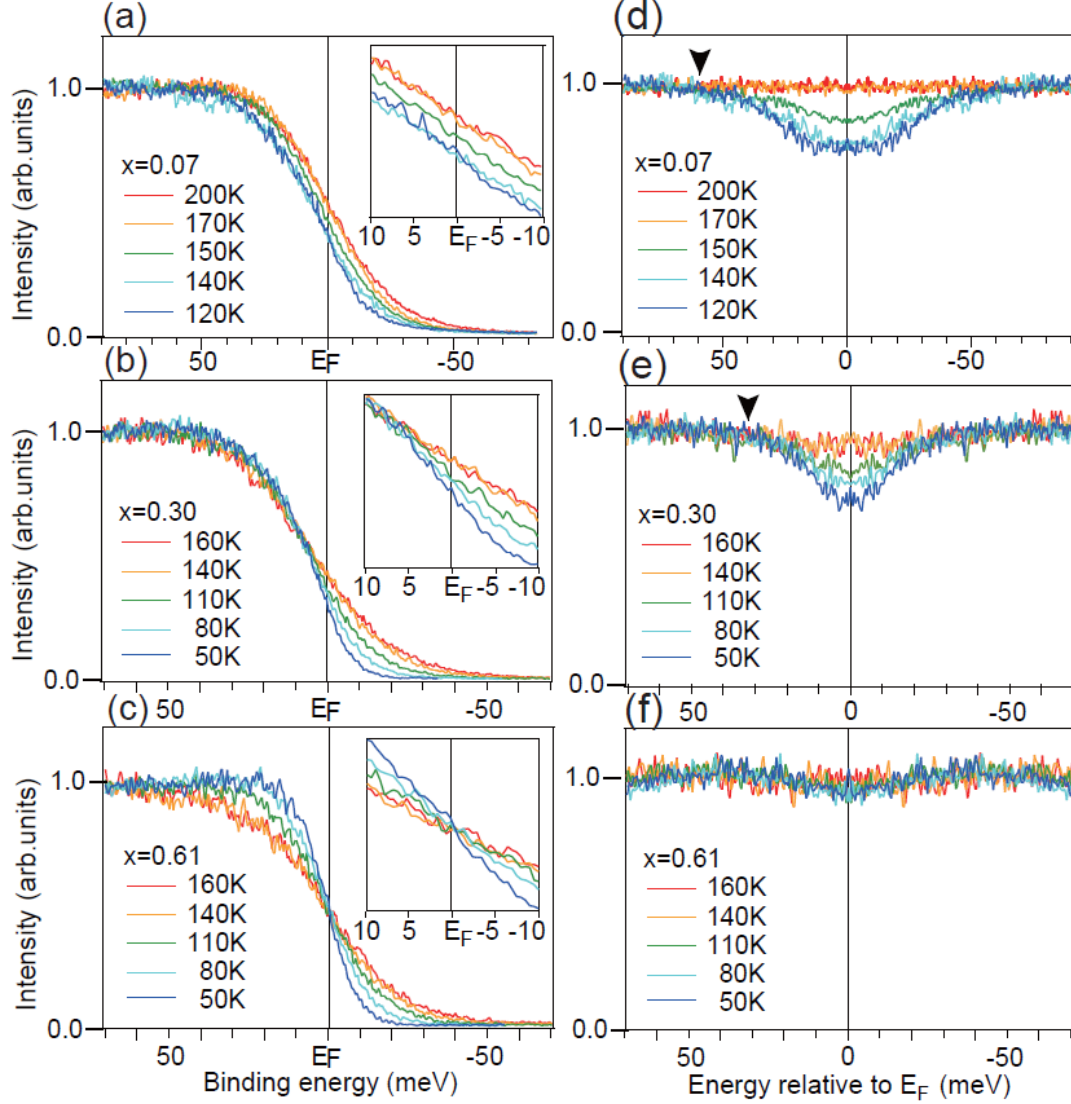


Fig. 3. (a-c) T -dependence of the EDCs at the k_F of the outer hole band measured for $x = 0.07$, 0.30 and 0.61 , respectively. Inset shows the spectra near the E_F in an enlarged energy scale. (d-f) EDCs symmetrized with respect to E_F and further normalized by the smoothed EDC at the highest- T . Black arrow indicates the crossing point of the spectra with decreasing T , representing the PG energy. Note the larger x-axis energy scale for $x = 0.07$ (panels (a) and (d)).

It is clear that the PG persists up to $T_{PG}^* \sim 180$ K for $x = 0.00$ ($T_{N,s} = 136$ K), ~ 160 K for 0.07 ($T_{N,s} = 114$ K) and ~ 110 K for 0.24 ($T_{N,s} = 55$ K), as indicated by the spectra in the light blue area of Fig. 4(a-c). This is indicative of a PG phase extending much above $T_{N,s}$. We note that the gapped area below $T_{N,s}$ can be also affected by the orbital-dependent band shift and/or the band folding due to the AF spin ordering transition. Actually, the gapped feature below $T_{N,s}$ show some additional fine structures (see the spectra in blue-shaded area of Fig. 4(a-c)). We thus focus on the PG formation considering the paramagnetic tetragonal T -region of $T_{N,s} < T < T_{PG}^*$, for the underdoped region of $0.00 \leq x \leq 0.24$. The PG is still observed for further doped $x = 0.3$ and 0.45 where the magneto-structural

transition no longer exists, but eventually disappears at $x = 0.61$, at least above 10 K. In Fig. 4(g-l), we plot the T -dependence of the gapped area S as a measure of PG formation, which is estimated by integrating the black area in Fig. 4(a-f). T_{PG}^* estimated from the onset T of the PG formation are plotted onto the phase diagram in Fig. 1. The obtained phase diagram of AsP122 clearly shows a PG phase extending above $T_{N,s}$ and T_c in a wide range of $0.00 \leq x < 0.61$.

Recent torque magnetometry and X-ray diffraction measurements reported that two-fold symmetric properties in the lattice and magnetic response appear at T_{Nem}^* ($> T_{N,s}$) [27]. Two-fold oscillation amplitudes of the torque for $x = 0.00$ and 0.23 are superimposed on Fig. 4(g) and 4(i), respectively. The.

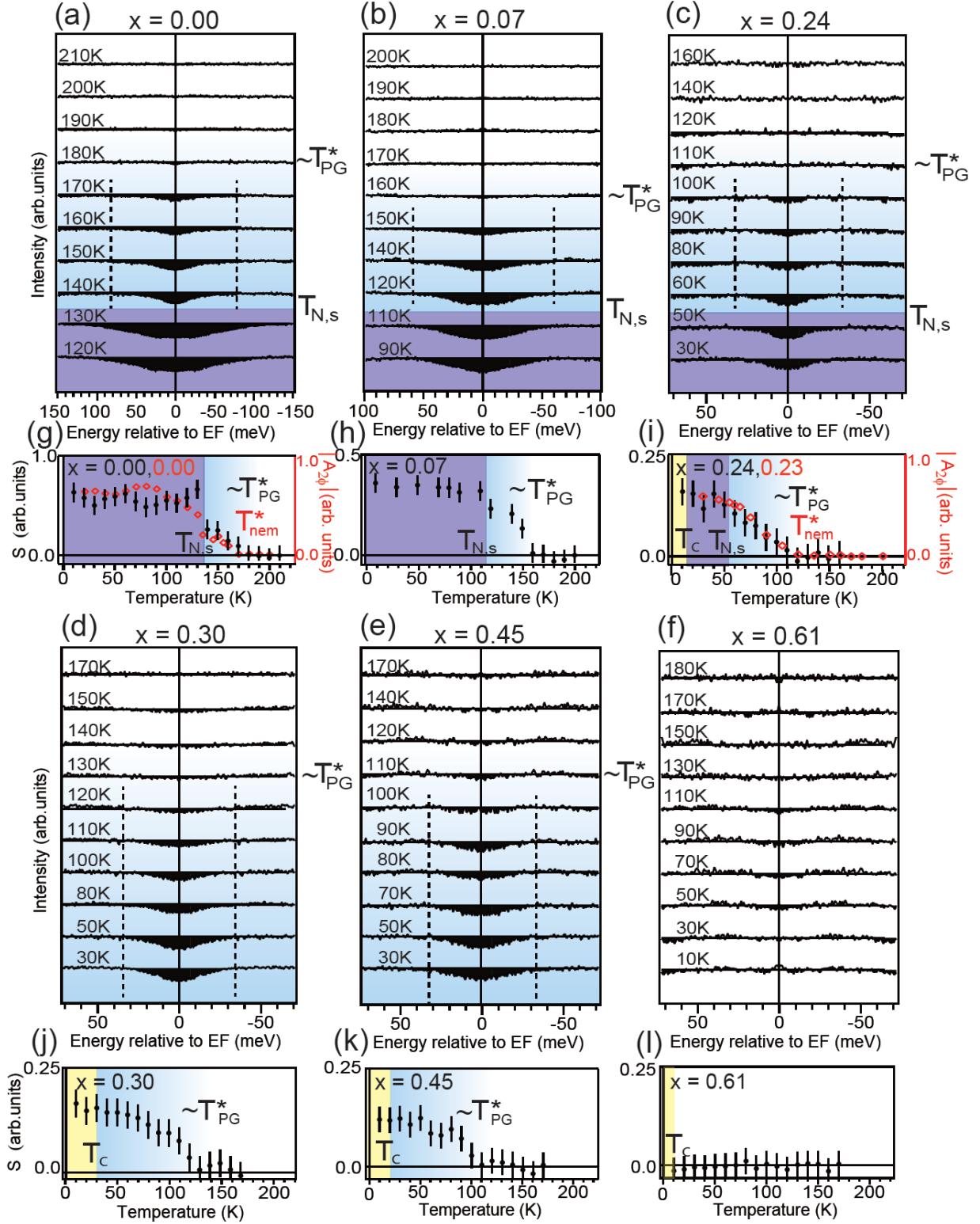


Fig. 4. (a-f) Symmetrized and normalized EDCs for $x = 0.00, 0.07, 0.24, 0.30, 0.45$ and 0.61 , respectively. The T -dependent depression of the spectral weight is indicated by the black shaded area. Note the larger x-axis energy scale for $x = 0.0$ and 0.07 (panels (a) and (b)). Dotted lines indicate pseudogap energy. (g-l) T -dependence of S , the gapped area. T_{PG}^* is defined by the temperature at which S starts to evolve. Though S can be also affected by the modification of the electronic structure across $T_{N,s}$, we clearly observe the PG above $T_{N,s}$ for $x = 0.00, 0.07$ and 0.24 . Two-fold oscillation amplitudes of the torque for $x = 0.00$ and 0.23 [27] are superimposed in (g) and (i), respectively. Background of each panel is colored in light blue for $T_{N,s} < T < T_{PG}^*$, blue for $T_c < T < T_{N,s}$ and yellow for $T < T_c$.

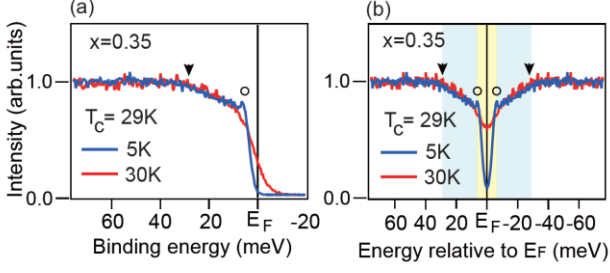


Fig. 5. (a) The EDCs measured at 5 K ($T < T_c$) and 30 K ($T_c < T$) for $x = 0.35$ by laser-ARPES ($h\nu = 6.994$ eV). Black arrow and open circle represent the energy position of PG and SC gap, respectively. (b) The EDCs symmetrized with respect to E_F . Light blue and yellow area highlight the energy scale of the PG and SC gap, respectively.

good correspondence between T_{Nem}^* and T_{PG}^* in Fig. 4(g) and 4(i) (also in Fig. 1) reveals that such electronic nematic phase is closely related to the PG observed by laser-ARPES, especially in the under-doped region.

The energy scale of the PG, Δ_{PG} , can be also estimated from the crossing point of the symmetrized EDCs as indicated by the black arrows in Fig. 3(d) and (e). It indicates that the PG tends to decrease from $\Delta_{PG} \sim 60$ meV to $\Delta_{PG} \sim 30$ meV with increasing P concentration from $x = 0.07$ to $x = 0.30$. Here we discuss energy scales of the PG and SC gaps in AsP122 system. EDCs below and above T_c for $x = 0.35$ are shown in Fig. 5(a). Both EDCs show broad hump structure around 30 meV (black arrow), indicative of the PG formation. In addition, SC gap appears around 5 meV with small coherent peak (open circle) in the EDC below T_c . Symmetrization of the EDCs in Fig. 5(b) clearly demonstrates that the PG energy is much larger than SC gap size in AsP122.

Synchrotron-based ARPES reveals that the hump structure in the EDCs are similarly found in the other hole FSs around BZ center. k_F positions measured by photons of $h\nu = 16 - 38$ eV are superimposed on the schematic FSs in Fig. 6(a). Symmetrized EDCs shown in Fig. 6 (b) were taken at k_F of different k_z values in inner hole FS for $x = 0.30$ below T_c , by using circular polarization. Note that the spectral intensity of the EDCs at k_F in inner hole band is not affected by other hole bands, even though it is not separately observed owing to the linear polarization. The hump structures ranging from 18 meV to 30 meV (black arrows) are signatures of the PG formation and observed at any k_z position. In particular, the shoulder structure around 5 - 8 meV (open circles) indicates SC gap opening, consistent with previous ARPES measurements [46,47,50]. Synchrotron-based ARPES thus show that SC gap in AsP122 is smaller than PG, consistent with laser-ARPES. PG

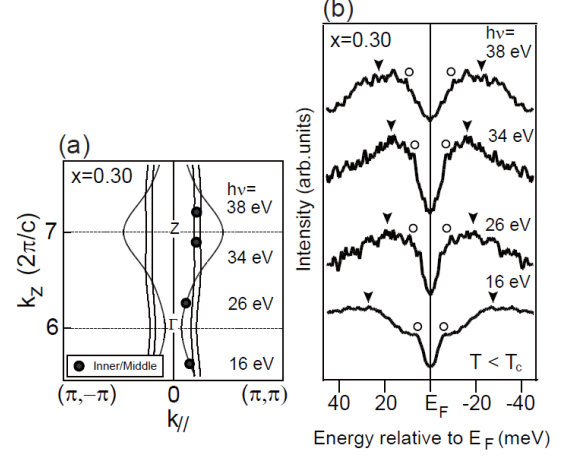


Fig. 6. (a) Schematics of three hole FSs for $x = 0.30$. k_F positions in inner hole FS are plotted by filled circles. (b) Symmetrized EDCs taken at k_F in inner hole FS for $x = 0.30$ below T_c by using photons of $h\nu = 16$ eV to 38 eV. Note that inner and middle hole FSs are nearly degenerate in the momentum region near Z plane. Black arrows and open circles represent the energy scale of the PG and SC gap, respectively.

with an energy scale higher than SC gap has been also reported for a variety of iron-based superconductors by several experimental probes [32,33,35,36,39,40]. Difference in energy scales of the PG and SC gaps in several hole FSs imply that the PG formation is not simply a precursor of the SC electron pairing [4-6].

One of the possible origins of the electronic nematicity is the rotational symmetry breaking induced by the orbital inequivalency. Indeed, the lifting of yz and zx orbital degeneracy in the band structure at tetragonal BZ corner had been discussed in a previous ARPES study on $\text{Ba}(\text{Fe}, \text{Co})_2\text{As}_2$ (FeCo122) [15]. Owing to the detwinning technique and polarization-dependent measurements, upper and lower hole-bands below E_F were separately observed at $(\pi, -\pi)$ point and (π, π) point, indicating zx and yz character, respectively [15]. Such inequivalent shift in the energy of zx/yz orbitals were observed even above $T_{N,s}$, implying the development of the zx/yz orbital order from high T . The recent X-ray absorption measurements on FeCo122 system also reported the differences in occupation of zx/yz orbitals above $T_{N,s}$ [30].

It is thus important to directly confirm the orbital inequivalency in AsP122, where the existence of both PG phase and electronic nematic phase has become clear. Since the detwinning by uniaxial pressure is known to raise the onset T of the anisotropy [15,51], here we chose twinned crystals to precisely compare with the $T - x$ phase diagram of PG. Previous

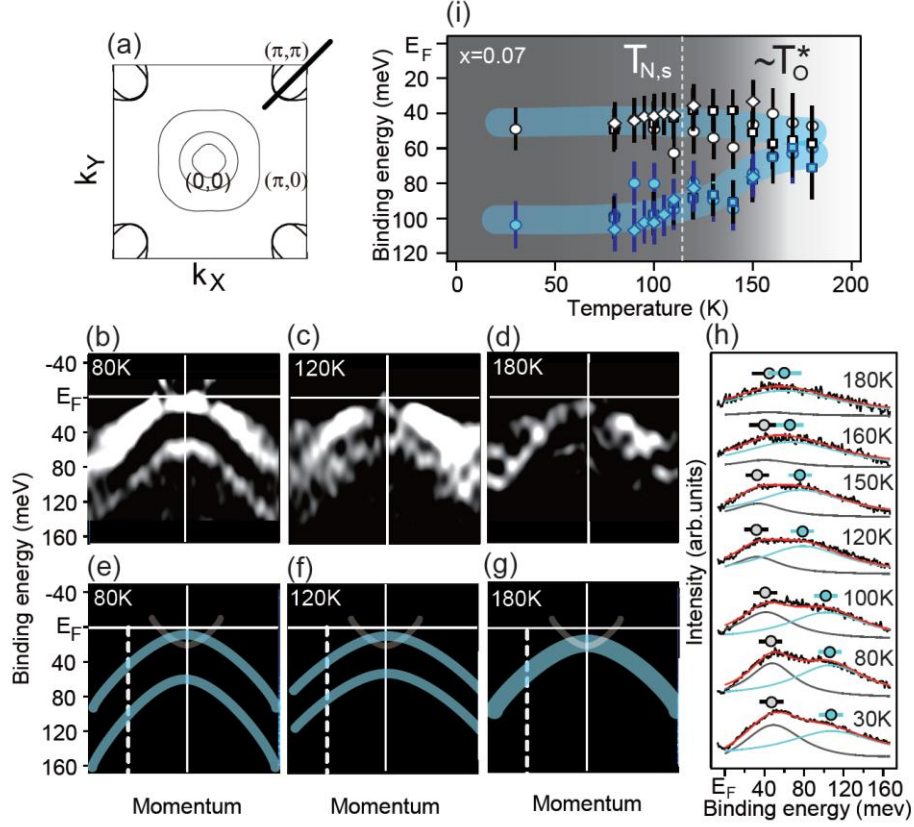


Fig. 7. (a) Schematics of the in-plane cut of Fermi surface sheets in Z plane of BaFe₂(As,P)₂. Black bar indicates the momentum region measured by helium-lamp ARPES for $x = 0.07$. (b) Band dispersion (second derivative) at BZ corner near Z plane measured by the photons of $h\nu = 40.8$ eV at 80 K ($T < T_{N,s}$). (c) The same measured at 120 K ($T_{N,s} < T < T_{PG}^*$). (d) The same measured at 180 K ($T_{PG}^* < T$). (e-g) Schematics of the band dispersions corresponding to (b-d), respectively. Two hole-bands (light blue curves) and weak-intensity electron-band (white curve) are observed at low- T . (h) T -dependence of the EDCs divided by FD function at the momentum cut indicated by the broken white line in (e-g). Linear background was subtracted from each spectrum. Red curves represent the fitting functions composed of double Lorentz functions illustrated by gray and light blue curves. Gray and light blue circles represent the peak positions in the EDCs obtained by the fitting procedure, indicating the energy position of upper and lower hole-band, respectively. (i) T -dependence of the energy position of the two hole-bands. Gray and light blue symbols represent the peak positions in the EDCs along a white broken line in (e-g) for upper and lower hole-bands, respectively. Circles, diamonds and squares represent the data obtained from different samples. Critical temperature T_{PG}^* where the two hole-bands start to shift is estimated to be 160 K ~ 180 K.

ARPES study confirmed that AsP122 has two electron bands forming FSs around BZ corner [45]. Along the momentum cut in Fig. 7(a), photoelectron intensity of those electron bands are relatively weak due to the matrix element effect. We thus chose this experimental geometry in order to emphasize the zx/yz hole bands just below E_F around BZ corner. Shown in Fig. 7(b-d) are the band dispersions (second derivative) at the tetragonal BZ corner near Z plane (along the momentum cut indicated in Fig. 7(a)) for $x = 0.07$ measured at 80 K, 120 K and 180 K, respectively. Two hole bands are clearly observed below E_F in the ARPES image at 80 K ($T < T_{N,s}$) in Fig. 7(b) (see also Fig. 7(e)). Note that the zx/yz hole bands below E_F at $(\pi, -\pi)$ and (π, π) are overlapped with each other because of the twinned domains. Importantly, the hole bands remain well separated

even at 120 K ($T_{N,s} < T < T_{PG}^*$) (Fig. 7(c) and (f)). At 180 K ($T_{PG}^* < T$), such a clear separation is not observed, indicating that the two bands are degenerate within experimental accuracy (see Fig. 7(d) and (g)).

Focusing on the energy positions of the two hole-bands, we investigated the T -dependence of the EDCs at a certain momentum indicated by the broken white lines in Fig. 7(e-g). We plotted the EDC peak positions from 30 K to 180 K by fitting them using double Lorentz functions as shown in Fig. 7(h). EDCs were divided by FD functions and linear background was subtracted from each spectrum. Two peaks are marked by black (upper hole-band) and light blue (lower hole-band) circles. Difference in energy between upper and lower hole-bands decreases as T increases as summarized in Fig.

7(i). While two hole-bands are well separated at low T , they become nearly degenerate around 160 -180 K. The observation of the nearly degenerate bands splitting into two hole-bands at BZ corner on cooling thus corresponds to the T -dependent inequivalent energy shift in zx/yz orbitals possibly related to orbital ordering, as was predicted theoretically [20-22]. We find that the inequivalent energy shift in zx/yz orbitals sets in around $T_O^* \sim 160 \text{ K} - 180 \text{ K}$ *i.e.* at a temperature nearly comparable to T_{Nem}^* and T_{PG}^* . This result indicates that the rotational symmetry breaking accompanying the PG formation in AsP122 occurs not only in the lattice and magnetism, but also in the orbital.

In this work, we found the PG phase well above $T_{N,s}$ and T_c in AsP122. The PG appears at the critical temperature comparable to the electronic nematic phase transition temperature where the rotational symmetry of the tetragonal electronic fluid is spontaneously broken [27]. In cuprates, ARPES measurements reported the PG formation temperature above the SC dome [52]. There it has been suggested that the appearance of the electronic nematicity is associated with the PG formation by neutron scattering [53], STM [54] and Nernst effect [6] measurements. Therefore our results indicate that the PG phase and the electronic nematicity appear to be common features of high- T_c superconductivity, both in cuprates and iron-pnictides.

However, there is a crucial difference between the two systems. In AsP122, the inequivalent energy shift in zx/yz orbitals is observed below $T_O^* \sim T_{PG}^* \sim T_{Nem}^*$ for $x = 0.07$ (Fig. 1 and 7(i)). This implies that the origin of the PG formation is likely to be linked to the orbital ordering. Note that since the zx/yz orbital inequivalency breaks the in-plane (xy) four-fold rotational symmetry, this is consistent with the reported nematicity, which exhibits only a two-fold rotational symmetry [27]. We stress that this mechanism is not applicable to cuprates composed of a single $d_{x^2-y^2}$ -orbital.

The degeneracy lifting in zx/yz orbitals near E_F should modify the electron scattering channels between the BZ center and corners, thereby making (π, π) and $(\pi, -\pi)$ inter-band scattering no longer equivalent. It may give rise to the anisotropic spin and/or orbital fluctuations causing the PG formation. Similar situation has been also theoretically discussed in nematic phase [55, 56]. Complex coupling of spin, orbital and lattice for respective compounds should be taken into account for further quantitative comparison.

It is notable that PG phase in AsP122 is robust over the superconducting phase. On the contrary, PG of BaKFe₂As₂

(BaK122) which was reported for under-doped $x = 0.25$ [41] has not been found in optimal doping so far. Although the PG phase in BaK122 is still not completely established, it may indicate that the PG phase of BaK122 is much more suppressed than AsP122.

Possible variety of the PG phase in BaFe₂As₂ (Ba122) family can be consistently classified in relation to the electronic nematic phase. Actually, nearly isotropic inplane electronic resistivity is reported in under-doped BaK122 [57,58], indicative of the small contribution of the electronic nematicity. At least in Ba122 family, a close relationship between PG formation and electronic nematic phase is now clarified although it seems to strongly depend on the character of the dopant ions. Understanding how the PG formation and orbital inequivalency reported here influence the normal state physical properties, which in turn should affect the variety of the superconducting gap symmetry in iron-based superconductors, is therefore a pressing issue, which deserves comprehensive studies of high- T_c superconductivity.

Acknowledgement: We acknowledge H. Kontani, S. Onari, M. Ogata, K. Ishida and R. Arita, for valuable discussions. We thank T. Kiss for experimental support. Synchrotron-based ARPES experiments were carried out at BL-9B at HiSOR (Proposal No. 10-B-27 and 11-B-1) and BL-28A at Photon Factory (Proposal No. 2009S2-005, No. 2012S2-001, and No. 2012G075).

* Correspondence and requests for materials should be addressed to T.S. (shimajima@ap.t.u-tokyo.ac.jp)

- [1] T. Timusk, & Statt, B., The PG in high-temperature superconductors: an experimental survey, *Rep. Prog. Phys.* **62**, 61 (1999).
- [2] M. R. Norman, D. Pines, and C. Kallin, *The pseudogap : friend or foe of high T_c ?* *Advances in Physics*, **54**, 715 (2005).
- [3] S. Hufner, M. A. Hossain, A. Damascelli, and G. A. Sawatzky, *Two gaps make a high-temperature superconductor?* *Rep. Prog. Phys.* **71**, 062501 (2008).
- [4] M. Randeria, *Proceedings of the International School of Physics "Enrico Fermi" Course CXXXVI on High Temperature Superconductors*, edited by Iadonisi, G., Schrieffer, J. R. & Chialfalo, M.L., (IOS Press, Amsterdam, 1999), p. 53.
- [5] V. Emery, and S. Kivelson, *Importance of phase fluctuations in superconductors with small superfluid density*, *Nature* **374**, 434 (1995).

- [6] R. Daou, *et al.* *Broken rotational symmetry in the PG phase of a high- T_c superconductor.* Nature **463**, 519 (2010).
- [7] J. E. Hoffman *et al.*, *A Four Unit Cell Periodic Pattern of Quasi-Particle States Surrounding Vortex Cores in $\text{Bi}_2\text{Sr}_2\text{CaCu}_2\text{O}_{8-\delta}$* Science **295**, 466 (2002).
- [8] M. Vershinin *et al.*, *Local Ordering in the PG State of the High- T_c Superconductor $\text{Bi}_2\text{Sr}_2\text{CaCu}_2\text{O}_8$* , Science **303**, 1995 (2004).
- [9] C. Howald, H. Eisaki, N. Kaneko, M. Greven, and A. Kapitulnik, *Periodic density-of-states modulations in superconducting $\text{Bi}_2\text{Sr}_2\text{CaCu}_2\text{O}_{8-\delta}$* Phys. Rev. B **67**, 014533 (2003).
- [10] J. G. Bednorz, and K. A. Muller, *Possible high T_c superconductivity in the Ba-La-Cu-O system*, Z. Phys. B **64**, 189 (1986).
- [11] Y. Kamihara, T. Watanabe, M. Hirano, and H. Hosono, *Iron-Based Layered Superconductor $a[\text{O}_{1-x}\text{F}_x]\text{FeAs}$ ($x = 0.05-0.12$) with $T_c = 26$ K*, J. Am. Chem. Soc. **130**, 3296 (2008).
- [12] C. de la Cruz *et al.*, *Magnetic order close to superconductivity in the iron-based layered $\text{LaO}_{1-x}\text{F}_x\text{FeAs}$ systems*, Nature **453**, 899 (2008).
- [13] D. J. Singh, and M. -H. Du, *Density Functional Study of $\text{LaFeAsO}_{1-x}\text{F}_x$ A Low Carrier Density Superconductor Near Itinerant Magnetism*, Phys. Rev. Lett. **100**, 237003 (2008).
- [14] T. Shimojima *et al.*, *Orbital-Dependent Modifications of Electronic Structure across the Magnetostructural Transition in BaFe_2As_2* , Phys. Rev. Lett. **104**, 057002 (2010).
- [15] M. Yi *et al.*, *Symmetry-breaking orbital anisotropy observed for detwinned $\text{Ba}(\text{Fe}_{1-x}\text{Co}_x)_2\text{As}_2$ above the spin density wave transition*, PNAS **108**, 6878 (2011).
- [16] I. I. Mazin, D. J. Singh, M. D. Johannes, and M. H. Du, *Unconventional Superconductivity with a Sign Reversal in the Order Parameter of $\text{LaFeAsO}_{1-x}\text{F}_x$* , Phys. Rev. Lett. **101**, 057003 (2008).
- [17] K. Kuroki *et al.*, *Unconventional Pairing Originating from the Disconnected Fermi Surfaces of Superconducting $\text{LaFeAsO}_{1-x}\text{F}_x$* , Phys. Rev. Lett. **101**, 087004 (2008).
- [18] H. Kontani, and S. Onari, *Orbital-Fluctuation-Mediated Superconductivity in Iron Pnictides: Analysis of the Five-Orbital Hubbard-Holstein Model*, Phys. Rev. Lett. **104**, 157001 (2010).
- [19] Y. Yanagi, Y. Yamakawa, and Y. Ōno, *Two types of s-wave pairing due to magnetic and orbital fluctuations in the two-dimensional 16-band d-p model for iron-based superconductors*, Phys. Rev. B **81**, 054518 (2010).
- [20] F. Kruger, S. Kumar, J. Zaanen, and J. V. Brink, *Spin-orbital frustrations and anomalous metallic state in iron-pnictide superconductors*, Phys. Rev. B **79**, 054504 (2009).
- [21] W. Lv, J. Wu, and P. Phillips, *Orbital ordering induces structural phase transition and the resistivity anomaly in iron pnictides*, Phys. Rev. B **80**, 224506 (2009).
- [22] C. Lee, W. -G. Yin, and W. Ku, *Ferro-Orbital Order and Strong Magnetic Anisotropy in the Parent Compounds of Iron-Pnictide Superconductors*, Phys. Rev. Lett. **103**, 267001 (2009).
- [23] J.-H. Chu *et al.*, *In-Plane Resistivity Anisotropy in an Underdoped Iron Arsenide Superconductor*, Science **329**, 824 (2010).
- [24] M. Nakajima *et al.*, *Unprecedented anisotropic metallic state in undoped iron arsenide BaFe_2As_2 revealed by optical spectroscopy*, PNAS **108**, 12238 (2011).
- [25] T.-M. Chuang *et al.*, *Nematic Electronic Structure in the "Parent" State of the Iron-Based Superconductor $\text{Ca}(\text{Fe}_{1-x}\text{Co}_x)_2\text{As}_2$* , Science **327**, 181 (2010).
- [26] J. Zhao *et al.*, *Spin waves and magnetic exchange interactions in CaFe_2As_2* , Nature Physics **5**, 555 (2009).
- [27] S. Kasahara *et al.*, *Electronic nematicity above the structural and superconducting transition in $\text{BaFe}_2(\text{As}_{1-x}\text{P}_x)_2$* , Nature **486**, 382 (2012).
- [28] M. Yi *et al.*, *Electronic reconstruction through the structural and magnetic transitions in detwinned NaFeAs* , New J. Phys. **14**, 073019 (2012).
- [29] Y. Zhang *et al.*, *Symmetry breaking via orbital-dependent reconstruction of electronic structure in detwinned NaFeAs* , Phys. Rev. B **85**, 085121 (2012).
- [30] Y. K. Kim *et al.*, *Existence of Orbital Order and its Fluctuation in $\text{Ba}(\text{Fe}_{1-x}\text{Co}_x)_2\text{As}_2$ Revealed by X-ray Absorption Spectroscopy*, arXiv:1112.2243
- [31] S. Kasahara *et al.*, *Evolution from non-Fermi- to Fermi-liquid transport via isovalent doping in $\text{BaFe}_2(\text{As}_{1-x}\text{P}_x)_2$ superconductors*, Phys. Rev. B **81**, 184519 (2010).
- [32] Y. Ishida *et al.*, *Unusual Pseudogap Features Observed in Iron Oxypnictide Superconductors*, J. Phys. Soc. Jpn. **77**, Suppl. C 61 (2008).
- [33] T. Sato *et al.*, *Doping Dependence of Pseudogap in $\text{LaFeAsO}_{1-x}\text{F}_x$* , J. Phys. Soc. Jpn. **77**, Suppl. C 65 (2008).
- [34] K. Ahilan *et al.*, *^{19}F NMR investigation of the iron pnictide superconductor $\text{LaFeAsO}_{0.89}\text{F}_{0.11}$* , Phys. Rev. B **78**, 100501R (2008).
- [35] D. R. Garcia *et al.*, *Core-level and valence-band study using angle-integrated photoemission on $\text{LaFeAsO}_{0.9}\text{F}_{0.1}$* , Phys. Rev. B **78**, 245119 (2008).

- [36] T. Mertelj *et al.*, *Distinct Pseudogap and Quasiparticle Relaxation Dynamics in the Superconducting State of Nearly Optimally Doped $\text{SmFeAsO}_{0.8}\text{F}_{0.2}$ Single Crystals*, Phys. Rev. Lett. **102**, 117002 (2009).
- [37] M. A. Tanatar *et al.*, *Pseudogap and its critical point in the heavily doped $\text{Ba}(\text{Fe}_{1-x}\text{Co}_x)_2\text{As}_2$ from c -axis resistivity measurements*, Phys. Rev. B **82**, 134528 (2010).
- [38] S. -H. Baek *et al.*, *PG-like phase in $\text{Ca}(\text{Fe}_{1-x}\text{Co}_x)_2\text{As}_2$ revealed by ^{75}As NQR*, Phys. Rev. B **84**, 094510 (2011).
- [39] Y. -C. Wen *et al.*, *Gap Opening and Orbital Modification of Superconducting FeSe above the Structural Distortion*, Phys. Rev. Lett. **108**, 267002 (2012).
- [40] S. J. Moon *et al.*, *Infrared Measurement of the Pseudogap of P-Doped and Co-Doped High-Temperature BaFe_2As_2 Superconductors*, Phys. Rev. Lett. **109**, 027006 (2012).
- [41] Y. -M. Xu *et al.*, *Fermi surface dichotomy of the superconducting gap and PG in underdoped pnictides*, Nat. Commun. **2**, 392 (2011).
- [42] K. Ohgushi, and Y. Kiuchi, *Doping dependence of Hall coefficient and evolution of coherent electronic state in the normal state of the Fe-based superconductor $\text{Ba}_{1-x}\text{K}_x\text{Fe}_2\text{As}_2$* , Phys. Rev. B **85**, 064522 (2010).
- [43] M. Nakajima *et al.*, *Growth of $\text{BaFe}_2(\text{As}_{1-x}\text{P}_x)_2$ Single Crystals ($0 \leq x \leq 1$) by $\text{Ba}_2\text{As}_3/\text{Ba}_2\text{P}_3$ -Flux Method*, J. Phys. Soc. Jpn. **81**, 104710 (2012).
- [44] T. Kiss *et al.*, *A versatile system for ultrahigh resolution, low temperature, and polarization dependent Laser-angle-resolved photoemission spectroscopy*, Review of Scientific Instruments **79**, 023106 (2008).
- [45] T. Yoshida *et al.*, *Two-Dimensional and Three-Dimensional Fermi Surfaces of Superconducting $\text{BaFe}_2(\text{As}_{1-x}\text{P}_x)_2$ and Their Nesting Properties Revealed by Angle-Resolved Photoemission Spectroscopy*, Phys. Rev. Lett. **106**, 117001 (2011).
- [46] T. Shimojima *et al.*, *Orbital-Independent Superconducting Gaps in Iron-Pnictides*, Science **332**, 564 (2011).
- [47] T. Shimojima *et al.*, *Angle-resolved photoemission study on the superconducting iron-pnictides of $\text{BaFe}_2(\text{As,P})_2$ with low energy photons*, Solid State Communications **152**, 695(2012).
- [48] K. Suzuki, H. Usui, and K. Kuroki, *Possible Three-Dimensional Nodes in the \pm Superconducting Gap of $\text{BaFe}_2(\text{As}_{1-x}\text{P}_x)_2$* , J. Phys. Soc. Jpn. **80**, 013710 (2011).
- [49] S. Hüfner, Photoelectron Spectroscopy (Springer, Berlin) (2003).
- [50] T. Yoshida *et al.*, *Importance of both spin and orbital fluctuations in $\text{BaFe}_2(\text{As}_{1-x}\text{P}_x)_2$:Evidence from superconducting gap anisotropy*, arXiv:1301.4818.
- [51] Supporting Online Material of Ref. 23.
<http://www.sciencemag.org/content/329/5993/824/suppl/DC1>
- [52] A. Damascelli, Z. Hussain, and Z. -X. Shen, *Angle-resolved photoemission studies of the cuprate superconductors*, Rep. Prog. Phys. **75**, 473 (1999).
- [53] V. Hinkov *et al.*, *Electronic liquid crystal state in the high-temperature superconductor $\text{YBa}_2\text{Cu}_3\text{O}_{6.45}$* , Science **319**, 597, (2008).
- [54] M. J. Lawler *et al.*, *Intra-unit-cell electronic nematicity of the high- T_c copper-oxide PG states*, Nature **466**, 347 (2010).
- [55] R. M. Fernandes, A. V. Chubukov, J. Knolle, I. Eremin, and J. Schmalian, *Preemptive nematic order, PG, and orbital order in the iron pnictides*, Phys. Rev. B **85**, 024534 (2012).
- [56] R. M. Fernandes, and J. Schmalian, *Manifestations of nematic degrees of freedom in the magnetic, elastic, and superconducting properties of the iron pnictides*, Supercond. Sci. Technol. **25**, 084005 (2012).
- [57] J. J. Ying *et al.*, *Measurements of the Anisotropic In-Plane Resistivity of Underdoped FeAs-Based Pnictide Superconductors*, Phys. Rev. Lett. **107**, 067001 (2011).
- [58] E. C. Blomberg, *et al.*, *Sign-reversal of the in-plane resistivity anisotropy in hole-doped iron pnictides*, arXiv:1304.3490.